Exploration of SMM behavior of Ln2-complexes derived from thianaphthene-2-carboxylic acid

SCHOLARONE™
Manuscripts

ARTICLE

Exploration of SMM behavior of Ln$_2$-complexes derived from thianaphthene-2-carboxylic acid

Soumava Biswas,*[a] Leena Mandal,[b] Yongbing Shen,[b] and Masahiro Yamashita*[a,b,c]

Two lanthanide-based dinuclear complexes [Ln^{III}(L)$_3$(DMF)(H$_2$O)]$_2$, [Ln = Dy^{III} (**1**) / Tb^{III} (**2**)] derived from thianaphthene-2-carboxylic acid have been synthesized and characterized in details. Single-crystal XRD analyses confirm that the centro-symmetric discrete dimeric structures contain eight-coordinated lanthanide centres with biaugmented trigonal prism geometry in the complexes. Magnetic studies reveal the presence of antiferromagnetic interaction as well as thermal depopulation of stark sublevels with the decrease in temperature for both complexes whereas prominent field induced single-molecule magnet behavior was observed for **1**. Also, isostructural yttrium based complex (**3**) and dilute sample **1'** have been prepared for the magnetic dilution study. **1'**, magnetically dilute sample of complex **1**, shows combination of direct, Orbach and Raman relaxation processes with effective energy barrier, ΔE = 19.508 cm^{-1} and relaxation time, τ_o = 9.710 × 10^{-10} s.

Introduction

In the recent years, a tremendous research effort has been observed for the exploration of single molecule magnets (SMMs) because of their prospective applications in the high-density data storage technology, quantum computing, cryogenic magnetic refrigeration, molecular spintronics, fabrication of nanoscopic molecular devices etc.[1] The distinct magnetic bistability, as well as unique quantum effect, make the SMMs a special class of materials.[2] Generally, SMMs can show the blocking of magnetization for a long period of time due to the large anisotropic spin reversal energy barrier. For that, the presence of high spin ground state and intrinsic magnetic anisotropy are the prime criteria in a SMM.[2] Now the predominant use of lanthanide ions to design and construct SMMs reveals their exceptional magneto-chemical natures. The superiority of lanthanide-based SMMs lies in the unquenched orbital angular momentum, crystal field effect and single-ion anisotropy of lanthanide ions.[3] In this regards, some excellent lanthanide based SMMs have been reported so far.[4] In very recent times, Mills et al. reported a dysprosocenium complex showing magnetic hysteresis up to 60 K.[5] {[(Me$_3$Si)$_2$N]$_2$Tb (THF)}$_2$(μ–η^2:η^2-N$_2$)$^-$, one of the finest example of lanthanide based dinuclear SMMs showing magnetic blocking at 14 K, was reported by Long et al.[6] On the other hand, Tang et al. reported an equatorially coordinated erbium based mononuclear SMM.[7] The only SMM having blocking temperature above liquid nitrogen, dysprosium metallocene cation [(Cp^{iPr5})Dy(Cp*)]$^+$, was reported by Layfield et al.[8] However understanding the molecular magnetic behavior of lanthanide based ploynuclear system in terms of single ion anisotropy and exchange interaction is a complex problem till date.[9] For lanthanide ions, although crystal field splitting is the most important parameter which governs the single ion anisotropy, but the magnetic exchange often affects the magnetic relaxation making the scenario more complicated.[9] So in this sense, dinuclear lanthanide SMMs could be one of the best choices to find the synergy between single ion anisotropy and magnetic exchange interactions.[10] For example, Winpenny et al. explored the direct exchange between two lanthanide ion centers in dinuclear single molecule magnets.[11]

Now to enhance the applicability of SMMs for the real world spintronics applications, it is necessary to investigate the mutual effect of some inherent functionality. Precisely saying, interplay between electronic properties (conductivity) with magnetism might be the key focus.[12] So, introducing some π-electron rich organic donor moieties with lanthanide centers can serve the purpose specifically. Tetrathiafulvalene as well as its derivatives are the very well explored electron rich moieties to introduce various electronic effects in molecular systems.[13] On the other hand, benzothienobenzothiophene (BTBT) could also deliver promising electronic effect which is clearly evident from its potential usefulness as organic field-effect transistor materials.[14] However surprisingly little attempt was observed to combine benzothienobenzothiophene or similar kind of moieties with lanthanide ions till date.[15] In this regard, we have chosen Benzo [b] thiophene-2-carboxylic acid or Thianaphthene-2-carboxylic acid (HL) as an organic ligand to construct lanthanide based dinucelar SMMs. This work reveals the syntheses, structures and investigations of SMM properties for two new lanthanide dinuclear complexes with thianaphthene moiety.

[a.] WPI Research Center, Advanced Institute for Materials Research, Tohoku University, 2-1-1 Katahira, Aoba-ku, Sendai 980-8577, Japan. E-mail: biswassoumava@gmail.com
[b.] Department of Chemistry, Graduate School of Science, Tohoku University, 6-3 Aza-Aoba, Aramaki, Sendai 980-8578, Japan. Email: masahiro.yamashita.c5@tohoku.ac.jp
[c.] School of Materials and Engineering, Nankai University, Tianjin 300350, China
†Electronic Supplementary Information (ESI) available: Tables S1–S3 and Fig. S1–S14. CCDC 1914747–1914749 for **1**–**3**, respectively, contain the supplementary crystallographic data for this paper.

Experimental Section

Materials and physical measurements

All reagents and solvents were purchased from commercial sources and used as received. Elemental analyses (C, H and N) were performed at the Research and Analytical centre for Giant Molecules, Tohoku University. IR spectra of samples were acquired at room temperature with a JASCO FT/IR-4200 spectrophotometer. PXRD measurements were performed on a BRUKER D2 PHASER. Magnetic susceptibility measurements were conducted using a Quantum Design SQUID magnetometer MPMS- XL (Quantum Design, San Diego, CA, USA). Diamagnetic corrections were made with Pascal's constants for derived dc susceptibilities of all the samples.[16] AC measurements were performed with an ac field amplitude of 3 Oe. High frequency ac data was collected by PPMS MODEL 6000. A polycrystalline sample embedded in *n*-eicosane was used for the measurements. EDX analysis was performed by an EDAX system equipped with a HITACHI S-4300 Scanning Electron Microscope.

Syntheses

[Dy^{III}(L)$_3$(DMF)(H$_2$O)]$_2$ (1). A N,N-dimethylformamide (DMF) solution (4 mL) of DyCl$_3$·6H$_2$O (0.075 g, 0.2 mmol) was added to a DMF solution (8 mL) of HL (0.107 g, 0.6 mmol). The solution was then heated in a capped glass vial at 110°C for 24 h. The resulting clear pale yellow solution was cooled to room temperature, filtered and kept in a glass vial. After five days, white crystals suitable for X-ray measurements were collected by filtration and washed with cold DMF. Yield (based on Dy): 0.083 g (53%). Anal. calcd for C$_{60}$H$_{48}$N$_2$O$_{16}$S$_6$Dy$_2$: C, 45.89; H, 3.08; N, 1.78%. Found: C, 45.57; H, 3.21; N, 1.89%. IR (cm^{-1}): 3315(w), 3223(w), 1657(s), 1600(s), 1559(m), 1522(s), 1456(m), 1432(s), 1396(s), 1376(s), 1323(m), 1180(m), 1154(m), 1112(m), 1084(m), 869(m), 808(s), 778(s), 750(m), 726(s), 685(s) and 586(s).

[Tb^{III}(L)$_3$(DMF)(H$_2$O)]$_2$ (2). This complex was prepared following the similar procedure to that described for **1** except using Tb(NO$_3$)$_3$·6H$_2$O (0.091 g, 0.2 mmol) instead of DyCl$_3$·6H$_2$O. Yield (based on Tb): 0.086 g (55%). Anal. calcd for C$_{60}$H$_{48}$N$_2$O$_{16}$S$_6$Tb$_2$: C, 46.10; H, 3.09; N, 1.79%. Found: C, 45.82; H, 3.13; N, 1.94%. IR (cm^{-1}): 3312(w), 3223(w), 1656(s), 1597(s), 1560(m), 1521(s), 1457(m), 1434(s), 1394(s), 1377(s), 1322(m), 1180(m), 1154(m), 1111(m), 1084(m), 869(m), 807(s), 777(s), 750(m), 725(s), 684(s) and 585(s).

[Y^{III}(L)$_3$(DMF)(H$_2$O)]$_2$ (3). This complex was prepared following the similar procedure to that described for **1** except using YCl$_3$·6H$_2$O (0.061 g, 0.2 mmol) instead of DyCl$_3$·6H$_2$O. Yield (based on Y): 0.081 g (57%). Anal. calcd for C$_{60}$H$_{48}$N$_2$O$_{16}$S$_6$Y$_2$: C, 50.63; H, 3.40; N, 1.97%. Found: C, 50.48; H, 3.46; N, 2.15%. IR (cm^{-1}): 3324(w), 3225(w), 1660(s), 1604(s), 1560(m), 1522(s), 1456(m), 1434(s), 1396(s), 1377(s), 1322(m), 1179(m), 1153(m), 1111(m), 1083(m), 870(m), 809(s), 778(s), 749(m), 726(s), 687(s) and 583(s).

[Y^{III}$_x$Dy$_{(1-x)}$(L)$_3$(DMF)(H$_2$O)]$_2$, x=0.89 (1'). This sample was prepared following the similar procedure to that described for **1**

except using using YCl$_3$·6H$_2$O (0.054 g, 0.18 mmol) and DyCl$_3$·6H$_2$O (0.008 g, 0.02 mmol) instead of pure DyCl$_3$·6H$_2$O. The presence of Y^{III} and Dy^{III} ions in the complex was confirmed from EDX spectrum (Fig. S1) and the ratio of the same was confirmed from elemental analysis and $\chi_M T$ vs. T plot. (Fig. S2). Yield: 0.078 g (54%). Anal. calcd for C$_{60}$H$_{48}$N$_2$O$_{16}$S$_6$Y$_{1.78}$Dy$_{0.22}$: C, 50.06; H, 3.36; N, 1.95%. Found: C, 49.83; H, 3.40; N, 1.91%. IR (cm^{-1}): 3319(w), 3226(w), 1659(s), 1604(s), 1560(m), 1521(s), 1457(m), 1434(s), 1397(s), 1377(s), 1322(m), 1180(m), 1153(m), 1110(m), 1084(m), 869(m), 809(s), 778(s), 751(m), 726(s), 686(s) and 585(s).

Crystal structure determination

The crystallographic data of **1**–**3** are summarized in Table 1. Diffraction data were collected on a Rigaku Saturn 724+ CCD diffractometer with graphite monochromated Mo-Kα radiation (λ = 0.71073 Å). The data collection temperature was 120 K for **1**–**3**. Data processing was performed using the CrystalClear crystallographic software package.[17] The structures were solved by SIR-92[18] using direct methods and the structures were refined by full-matrix least-squares based on F^2 using SHELXL-2014/7[19] packages. C12 atom in each of the complexes **1**–**3** was disordered over two sites. The disorder was fixed allowing each atom to refine freely and the final occupancy parameters were set as: 0.9 and 0.1 for C12 in **1** and **3**; 0.85 and 0.15 for C12 in **2**. The hydrogen atoms were refined isotropically, while the non-hydrogen atoms were refined anisotropically. The final refinements converged at the *R1* values [I > 2σ(I)] 0.0509, 0.0765 and 0.0813 for **1**–**3**, respectively.

Results and discussion

Syntheses and characterization

Complexes **1**–**3** and **1'** were prepared by the reaction of HL and Ln-chloride / nitrate salt in 3:1 molar ratio in DMF at 110 °C. The powder X-ray diffraction pattern (PXRD) of the synthesized samples matched well with the simulated pattern for the single crystal data, which confirmed the phase purity of bulk sample (Fig. S3). The solid phase UV-VIS spectra of complex **1** were measured at room temperature (Fig S4). The presence of absorption band at 337 nm for both the complex **1** may be attributed to the π→π* transition of the ligand. The corresponding optical band gap is estimated to be 3.21 eV for complex **1** (Fig S4).

Description of crystal structures

Complexes **1**–**3** are iso-structural and crystallize in the monoclinic space group *P*2$_1$/*c* (Fig. 1). Selected bond lengths and bond angles in the coordination environment of the trivalent lanthanide / yttrium ions are listed in Table S1. The centro-symmetric discrete dimeric structures contain eight-coordinated lanthanide / yttrium centres that adopt a biaugmented trigonal prism geometry, determined by SHAPE 2.1[20] (Table S2). Four coordination positions of each lanthanide / yttrium ion are occupied by two η^2-chelating

Table 1 Crystallographic data for **1**−**3**

	1	2	3
Empirical formula	$C_{60}H_{48}N_2O_{16}S_6Dy_2$	$C_{60}H_{48}N_2O_{16}S_6Tb_2$	$C_{60}H_{48}N_2O_{16}S_6Y_2$
Formula weight	1570.36	1563.20	1423.18
Crystal system	Monoclinic	Monoclinic	Monoclinic
Space group	$P2_1/c$	$P2_1/c$	$P2_1/c$
a /Å	8.6584(17)	8.656(3)	8.683(3)
b /Å	25.153(5)	25.176(8)	25.161(8)
c /Å	14.150(3)	14.150(5)	14.182(5)
α /°	90	90	90
β /°	106.892(3)	106.742(4)	107.162(6)
γ /°	90	90	90
V /Å^3	2948.7(10)	2952.9(17)	2960.4(17)
Z	2	2	2
ρ_{calcd} /g cm^{-3}	1.769	1.758	1.597
λ (Mo K$_\alpha$)/Å	0.71073	0.71073	0.71073
μ /mm^{-1}	2.799	2.660	2.234
T /K	120(2)	120(2)	120(2)
$F(000)$	1556	1552	1448
2θ range for data collection /°	8.092–54.940	8.082–54.918	8.094–54.916
Index ranges	$-11 \leq h \leq 11$	$-10 \leq h \leq 11$	$-11 \leq h \leq 9$
	$-32 \leq k \leq 36$	$-31 \leq k \leq 32$	$-17 \leq k \leq 32$
	$-10 \leq l \leq 18$	$-8 \leq l \leq 18$	$-18 \leq l \leq 18$
No. measured reflections	11395	11580	15909
No. independent reflections	6427	6572	6579
R_{int}	0.0343	0.0460	0.0393
No. refined parameters	371	390	381
No. observed reflections, $I>2\sigma(I)$	4220	4565	4947
Goodness-of-fit on F^2, S	1.037	1.131	1.116
$R_1{}^a$, $wR_2{}^b$ [$I>2\sigma(I)$]	0.0509, 0.1357	0.0765, 0.1586	0.0813, 0.2211
$R_1{}^a$, $wR_2{}^b$ (all data)	0.0762, 0.1598	0.1114, 0.1813	0.1010, 0.2446

$^a R_1 = [\sum ||F_o| - |F_c||/\sum |F_o|]$. $^b wR_2 = [\sum w(F_o{}^2 - F_c{}^2)^2/\sum w(F_o{}^2)^2]^{1/2}$

carboxylates from L$^-$. Two lanthanide centres are bridged by two L$^-$ through μ-η^1: η^1-bidentate bridging mode of the carboxylate moieties and hence satisfy two coordination positions of each. Thus the +III charge of each lanthanide / yttrium centre is balanced entirely by coordinated thianaphthene- 2- carboxylates. The remaining two coordination sites of each lanthanide / yttrium ion are coordinated to two oxygen atoms provided by one water molecule and one N,N-dimethylformamide (DMF) molecule. The bonds involving the lanthanide / yttrium ions and bridging carboxylates are shorter than those involving the chelating carboxylates: the range of Ln^{III}/Y^{III}—O(carboxylate) bond distances for the chelating carboxylates is 2.375—2.511 Å in **1**–**3**, whereas for bridging carboxylates it is 2.252—2.362 Å. The Ln^{III}/Y^{III}—O(water) (2.355, 2.375 and 2.345 Å for **1**–**3,** respectively) and Ln^{III}/Y^{III}—O(DMF) (2.315, 2.319 and 2.294 Å for **1**–**3**, respectively) bond distances are also shorter than that for the chelating carboxylates.

The intra-molecular Ln^{III}····Ln^{III} or Y^{III}····Y^{III} separation is 4.551, 4.523 and 4.602 Å for **1**–**3**, respectively. The smallest value for intermolecular Ln^{III}····Ln^{III} separation is 6.304 and 6.319 Å for **1** and **2**, respectively, while that is 6.291 Å in case of the yttrium analogue, **3**. Presence of intermolecular π····π stacking interactions

are found in both complexes having the π···· π stacking distances 3.706, 3.713 and 3.708 Å for **1**–**3**, respectively (Fig. S5).

(a)

(b)
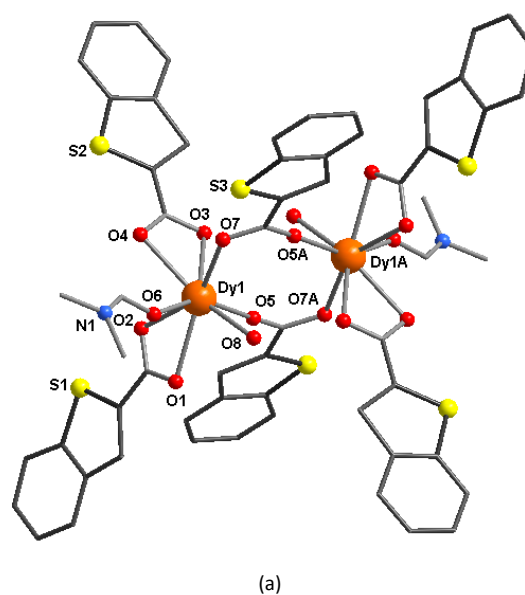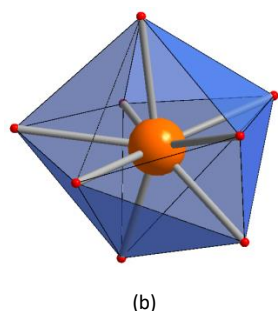
Fig. 1 (a) Crystal structure of **1**. Symmetry code: A, 2–x, 2–y, 1–z; (b) Polyhedral representation of the coordination environment around Dy^{III} centre.

In all complexes, one hydrogen atom of the coordinated water molecule participates in intra-molecular hydrogen bonding with one oxygen atom (O3) of one of the bidentate chelating carboxylates (Fig. S5). In this case, the D⋯A distance is 2.718, 2.713 and 2.743 Å for **1–3**, respectively. Another hydrogen atom of the water molecule involves in inter-molecular hydrogen bonding with one oxygen (O1) atom of a chelating carboxylate from neighboring dinuclear unit with the range of D⋯A distance of 2.772—2.785 Å for **1–3**.

Magnetic properties

For complexes **1** and **2**, the direct current (dc) magnetic susceptibility measurements were performed in the temperature range of 1.8–300 K at 1000 Oe on polycrystalline powdered samples. The room temperature $\chi_M T$ value of complex **1** is 28.61 cm^3 K mol^{-1} which is very close to the theoretical value (28.34 cm^3 K mol^{-1}, $^6H_{15/2}$, g = 4/3) for two uncoupled Dy^{3+} ions. With a decrease in temperature from 300 K, the $\chi_M T$ values slowly decrease upto around 80 K and after that suddenly decrease to a value of value of 18.59 cm^3 K mol^{-1} at 2K (Fig. 2). The overall shape of the $\chi_M T$ plot does not surely indicate the presence of antiferromagnetic interactions between dysprosium centers because of the large orbital angular momentum, strong spin–orbit coupling, and thermal depopulation of stark sublevels for dysprosium ions.[21]
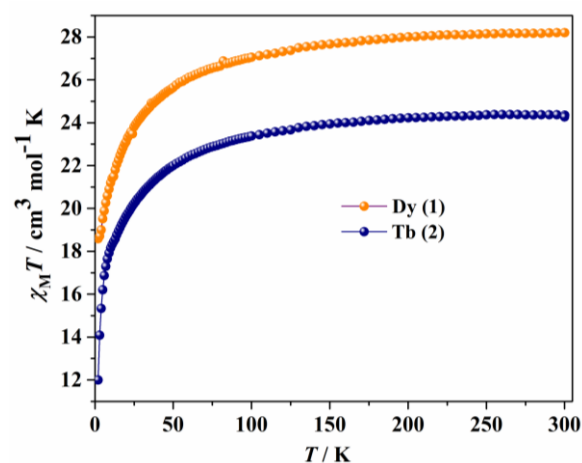
Fig. 2 Temperature dependence of the $\chi_M T$ products in 1000 Oe for complexes **1** and **2**

For complex **2**, the room temperature $\chi_M T$ value (24.53 cm^3 K mol^{-1}) is consistent with the theoretical value (23.63 cm^3 K mol^{-1}, $^7F_6$, g = 3/2) with two uncoupled terbium ions. In case of complex **2**, the $\chi_M T$ values slowly decrease with temperature to a value of 6.1 cm^3 K mol^{-1} at 25 K. After that the rapid decrease suggests small antiferromagnetic interaction with the depopulation of stark sublevels (Fig. 2).[21]

The isothermal magnetization measurements were performed for complexes **1** and **2** with the increasing magnetic field (0 Oe to 50 kOe) at 1.8 K. A sudden increase in the magnetization was observed for both the complexes at low field region, following onwards a slow gradual increase lead to the unsaturation at 50 kOe (Fig. S6). These experimental magnetization values (11.14 $N\mu_B$ for **1** and 9.21 $N\mu_B$ for **2** at 50 kOe) are smaller than the theoretical one. So the unsaturation in the magnetization measurements signifies the presence of magnetic anisotropy and/or low-lying excited states for both the complexes.[22]

The magnetic dynamics of complexes **1** and **2** were investigated by alternative current (ac) magnetic susceptibility measurements in order to analyse the occurrence of single molecule magnetic behavior or slow magnetic relaxations. For complex **1** (having a Kramers ion, Dy^{3+}), at first, no obvious peak maximum was observed in the out of phase ac susceptibility for a frequency range of 1-1000 Hz (under an oscillating ac field of 3 Oe) in the absence of external dc magnetic field (Fig. S7). The fast zero-field quantum tunneling of magnetization (QTM) might be responsible for the absence of frequency dependent peak maxima.[23] To find the optimized dc magnetic field for the suppression of QTM, ac magnetic susceptibility measurements were performed under several (0 Oe to 3000 Oe) dc magnetic fields at 1.85 K (Fig. S8). Now, an optimized field of 2600 Oe was chosen due to the appearances of peak maxima in low frequency region (Fig. 3). In presence of the optimized dc magnetic field, frequency dependent clear peak maxima were observed in out of phase ac susceptibility. However, the presence of multiple peak maxima in the out of phase ac susceptibility plot indicates some inter- and intra-molecular exchange or dipolar interactions in complex **1**.[24] To minimize such interactions, magnetically diluted complex, **1'**, with yttrium ion was synthesized in an approximately 1:9 molar ratio (see ESI for experimental details). A detail ac magnetic study was performed on this yttrium doped sample to evaluate the magnetic relaxation of dysprosium ion. However, because of fast QTM, no peak maxima were found in the out of phase ac susceptibility without dc field (Fig. S9). At an optimized dc magnetic field of 1000 Oe, clear single peak maxima were observed in the out-of phase susceptibility plot, implying the single molecule magnetic behavior of dysprosium ion in complex **1'** (Fig. S10 and Fig. 4). The ac susceptibility data were fitted with Cole-Cole model for the temperature range of 1.85–3.25 K (Fig. S11 and Table S3).[25] The range of the α values (0.33-0.40) indicates the broad distribution of magnetic relaxation in the low temperature region. So the temperature dependence of the magnetic relaxation could be the combination of several mechanisms, for which the following eqn (1) has been used to extract the energy barrier and relaxation time:

non-Kramers ion, Tb^{3+}), no frequency dependency was observed in the out of phase ac susceptibilities under the zero field as well as several applied dc magnetic fields (Fig. S7 and Fig. S14). So the
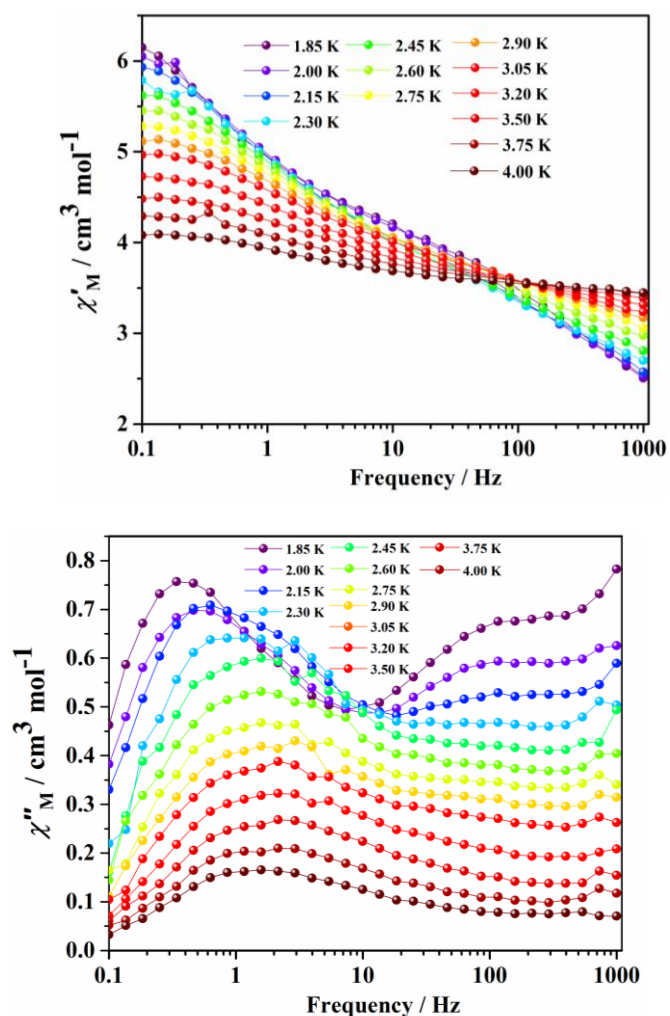
Fig.3 Frequency dependence of the in phase (above) and out of phase (below) components of the ac magnetic susceptibility for **1** under 2600 Oe dc field.

$$\tau^{-1} = AH^4T^n + CT^m + \tau_0^{-1}exp(-\Delta E/k_BT) + 1/QTM \qquad (1)$$

Where, the first term contributes for the direct process, second term denotes the Raman process, whereas the third and fourth term account for Orbach relaxation and QTM respectively.[3a, 24a, 26] The m value is found to be 9 for a Kramers ion, Dy^{3+}.[27] The fitting results suggest that the magnetic relaxations happen through a combination of competing direct, Raman and thermally assisted Orbach mechanism (Fig. 5). The anisotropic energy barrier is ΔE = 19.508 cm^{-1} with the pre-exponential factor (τ_0) = 9.710 × 10^{-10} s, consistent with proper SMM behavior. Additionally, only quantum tunnelling, direct contributions and Raman process have been taken into consideration to analyse temperature dependence of magnetic relaxation time (Fig. S12).

To inspect the magnetic relaxation for complex **1** in the high frequency region, we also performed the ac magnetic susceptibility measurements under (0 Oe to 3000 Oe) dc magnetic fields for a frequency range of 10-10000 Hz at 2 K. For an optimized field of 600 Oe, prominent peak maxima were observed in out of phase ac susceptibility in the range of 1.9 K to 5 K indicating the presence of slow magnetic relaxation (Fig. S13). For the complex **2** (having a

Fig. 4 Frequency dependence of the in phase (above) and out of phase (below) components of the ac magnetic susceptibility for **1'** under 1000 Oe dc field.
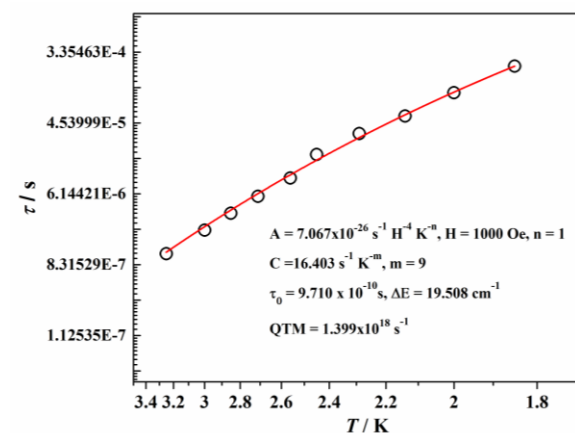
Fig. 5 Temperature dependence of relaxation time for **1'**.

splitting of integer J ground states by transverse anisotropy promotes the under-barrier magnetic relaxation mechanisms, namely the spin-parity effect, could lead to such non-SMM behavior.[21a, 28]

Conclusions

This work demonstrates the exploration of two new isostructural dinuclear lanthanide (Ln = Dy and Tb) complexes based on thianaphthene-2-carboxylic acid in terms of their structural features and molecular magnetic properties. An electron rich benzothiophen ligand is employed to introduce lanthanide based single molecule magnets. The static (dc) magnetic studies reveal a weak antiferromagnetic interaction as well as depopulation of stark sublevels in the lanthanide ions for both of the complexes. Whereas, the dynamic magnetic studies for complex **1** show that it exhibits field-induced slow relaxation of magnetization, consistent with typical SMM behavior. Also, isostructural yttrium based complex (**3**) and dilute sample **1'** have been synthesized for the magnetic dilution study of complex **1**. Notably for the magnetically dilute dysprosium complex, the magnetic relaxation dynamics is governed by Orbach as well direct and Raman relaxation processes. Therefore, it can be realized that the combination of lanthanide ions with benzothiophen based ligands can create interesting molecular magnetic materials which could have potential usefulness for spintronics research as well.

Conflicts of interest

There are no conflicts to declare.

Acknowledgements

Notes and references

1   (*a*) L. Bogani and W. Wernsdorfer, *Nature Mater*., 2008, **7**, 179; (*b*) N. Domingo, E. Bellido and D. Ruiz-Molina, *Chem. Soc. Rev*., 2012, **41**, 258; (*c*) M. Evangelisti, O. Roubeau, E. Palacios, A. Camón, T. N. Hooper, E. K. Brechin and J. J. Alonso, *Angew. Chem. Int. Ed*., 2011, **50**, 6606; (*d*) G. Aromí, D. Aguilá, P. Gamez, F. Luis and O. Roubeau, *Chem. Soc. Rev*., 2012, **41**, 537; (*e*) A. Candini, S. Klyatskaya, M. Ruben, W. Wernsdorfer and M. Affronte, *Nano Lett*. 2011, **11**, 2634; (*f*) S. Biswas, A. K. Mondal and S. Konar, *Inorg. Chem*., 2016, **55**, 2085.

2   (*a*) N. Ishikawa, M. Sugita, T. Ishikawa, S.-y. Koshihara and Youkoh Kaizu, *J. Am. Chem. Soc*., 2003, **125**, 8694; (*b*) D. N. Woodruff, R. E. P. Winpenny and R. A. Layfield, *Chem. Rev*., 2013, **113**, 5110; (*c*) A. Giusti, G. Charron, S. Mazerat, J.-D. Compain, P. Mialane, A. Dolbecq, E. Rivière, W. Wernsdorfer, R. N. Biboum, B. Keita, L. Nadjo, A. Filoramo, J.-P. Bourgoin, and T. Mallah, *Angew. Chem. Int. Ed*., 2009, **48**, 4949; (*d*) J. P. Costes, S. T. Padilla, I. Oyarzabal, T. Gupta, C. Duhayon, G. Rajaraman, E. Colacio, *Inorg. Chem*., 2016, **55**, 4428.

3   (*a*) S. T. Liddle and J. v. Slageren, *Chem. Soc. Rev.,* 2015, **44**, 6655; (*b*) K. Liu, X. Zhang, X. Meng, W. Shi, P. Cheng and A. K. Powell, *Chem. Soc. Rev*., 2016, **45**, 2423;. (*c*) L. Sorace, C. Benelli and D. Gatteschi, *Chem. Soc. Rev*., 2011, **40**, 3092.

4   P. Zhang, Y.-N. Guo and J. Tang, *Coord. Chem. Rev*., 2013, **257**, 1728.

5   C. A. P. Goodwin, F. Ortu, D. Reta, N. F. Chilton and D. P. Mills, *Nature*, 2017, **548**, 439.

6   (*a*) J. D. Rinehart, M. Fang, W. J. Evans and J. R. Long, *J. Am. Chem. Soc*., 2011, **133**, 14236; (*b*) J. D. Rinehart, M. Fang, W. J. Evans and J. R. Long, *Nat. Chem*., 2011, **3**, 538.

7   P. Zhang, L. Zhang, C. Wang, S. Xue, S.-Y. Lin and J. Tang, *J. Am. Chem. Soc*., 2014, **136**, 4484.

8   F.-S. Guo, B. M. Day, Y.-C. Chen, M.-L. Tong, A. Mansikkamäki and R. A. Layfield, *Science*, 2018, **362**, 1400.

9   (*a*) M. Guo, Y. Xu, J. Wu, L. Zhao and J. Tang, *Dalton Trans*., 2017, **46**, 8252; (*b*) L. Zhang, Y.-Q. Zhang, P. Zhang, L. Zhao, M. Guo and J. Tang, *Inorg. Chem*., 2017, **56**, 7882.

10 (*a*) F. Habib and M. Murugesu, *Chem. Soc. Rev.,* 2013, **42**, 3278; (*b*) I. F. Díaz-Ortega, J. M. Herrera, D. Aravena, E. Ruiz, T. Gupta, G. Rajaraman, H. Nojiri and E. Colacio, *Inorg. Chem*., 2018, **57**, 6362; (*c*) A. V. Gavrikov, N. N. Efimov, A. B. Ilyukhin, Z. V. Dobrokhotovaand and V. M. Novotortsev, *Dalton Trans*., 2018, **47**, 6199; (*d*) S. Ghosh, S. Mandal, M. K. Singh, C.-M. Liu, G. Rajaraman and S. Mohanta, *Dalton Trans.*, 2018, **47**, 11455.

11 (*a*) E. M. Pineda, N. F. Chilton, R. Marx, M. Dorfel, D. O. Sells, P. Neugebauer, S.-D. Jiang, D. Collison, J. V. Slageren, E. J. L. McInnes, R. E. P. Winpenny, *Nat. Commun*., 2014, **5**, 5243; (*b*) M. J. Giansiracusa, E. Moreno-Pineda, R. Hussain, R. Marx, M. M. Prada, P. Neugebauer, S. Al-Badran, D. Collison, F. Tuna, J. v. Slageren, S. Carretta, T. Guidi, E. J. L. McInnes, R. E. P. Winpenny and N. F. Chilton, *J. Am. Chem. Soc*., 2018, **140**, 2504.

12 (*a*) E. Coronado, J. R. Galán-Mascarós, Carlos J. Gómez-García and V. Laukhin, *Nature*, 2000, **408**, 447; (*b*) G. Cosquer, Y. Shen, M. Almeida and M. Yamashita, *Dalton Trans*., 2018, **47**, 7616.

13 (*a*) J. Su, T.-H. Hu, R. Murase, H.-Y. Wang, D. M. D'Alessandro, M. Kurmoo and J.-L. Zuo, *Inorg. Chem*., 2019, **58**, 3698; (*b*) T. T. d. Cunha, F. Pointillart, B. L. Guennic, C. L. M. Pereira, S. Golhen, O. Cador and L. Ouahab, *Inorg. Chem*., 2013, **52**, 9711; (*c*) L. Martin, *Coord. Chem. Rev*., 2018, **376**, 277; (*d*) F. Gao, X.-M. Zhang, L. Cui, K. Deng, Q.-D. Zeng and J.-L. Zuo, *Sci. Rep*., 2014, **4**, 5928.

14 (*a*) R. Janneck, N. Pilet, S. P. Bommanaboyena, B. Watts, P. Heremans, J. Genoe and C. Rolin, *Adv. Mater*., 2017, **29**, 1703864; (*b*) H. Ebata, T. Izawa, E. Miyazaki, K. Takimiya, M. Ikeda, H. Kuwabara and T. Yui, *J. Am. Chem. Soc*., 2007, **129**, 15732; (*c*) Y. Xiong, X. Qiao, H. Wu, Q. Huang, Q. Wu, J. Li, X. Gao and H. Li, *J. Org. Chem*., 2014, **79**, 1138; (*d*) P. Tisovský, A. Gáplovský, K. Gmucová, M. Novota, M. Pavúk and M. Weis, *Org. Electron*., 2019, **68**, 121.

15 (*a*) P. Y. Chen, M. Z. Wu, T. Li, X. J. Shi, L. Tian and Z. Y. Liu, *Inorg. Chem*., 2018, **57**, 12466; (*b*) R. Liu, Y. Ma, P. Yang, X. Song, G. Xu, J. Tang, L. Li, D. Liao and S. Yan, *Dalton Trans*., 2010, **39**, 3321; (*c*) T. Han, W. Shi, Z. Niu, B. Na and P. Cheng, *Chem. Eur. J.,* 2013, **19**, 994.

16 (*a*) G. A. Bain and J. F. Berry, *J. Chem. Educ*., 2008, **85**, 532; (*b*) O. Kahn, *Molecular Magnetism*, VCH, New York, 1993.

17 Crystal Clear-SM, 1.4.0 SP1; Rigaku Corporation: Tokyo, Japan, 17 April 2008.

18 A. Altomare, M. C. Burla, M. Camalli, G. L. Cascarano, C. Giacovazzo, A. Guagliardi, A. G. G. Moliterni, G. Polidori and R. Spagna, SIR97: A new tool for crystal structure determination and refinement, *J. Appl. Crystallogr*. 1999, **32**, 115.

19 G. M. Sheldrick, SHELXL-2014/7, Crystal Structure Refinement Program, University of Göttingen, 2014.

20 (*a*) S. Alvarez, P. Alemany, D. Casanova, J. Cirera, M. Llunell and D. Avnir, *Coord. Chem. Rev*., 2005, **249**, 1693; (*b*) J. Cirera, E. Ruiz and S. Alvarez, *Chem. Eur. J*., 2006, **12**, 3162.

21 (*a*) M. Ren, Z.-L. Xu, S.-S. Bao, T.-T. Wang, Z.-H. Zheng, R. A. S. Ferreira, L.-M. Zheng and L. D. Carlos, *Dalton Trans*., 2016, **45**, 2974; (*b*) Y. J. Gao, G. F. Xu, L. Zhao, J. K. Tang and Z. L. Liu, *Inorg. Chem*., 2009, **48**, 11495; (*c*) Y. N. Guo, G. F. Xu, W. Wernsdorfer, L. Ungur, Y. Guo, J. Tang, H. J. Zhang, L. F. Chibotaru and A. K. Powell, *J. Am. Chem. Soc*., 2011, **133**, 11948; (*d*) S. Biswas, H. S. Jena, S. Sanda and S. Konar, *Chem. Eur. J.*, 2015, **21**, 13793;. (*e*) P. P. Yang, X. F. Gao, H. B. Song, S. Zhang, X. L. Mei, L. C. Li and D. Z. Liao, *Inorg. Chem*., 2011, **50**, 720.

22 (*a*) M. Jeletic, P.-H. Lin, J. J. L. Roy, I. Korobkov, S. I. Gorelsky and M. Murugesu, *J. Am. Chem. Soc*., 2011, **133**, 19286; (*b*) F. Habib, P.-H. Lin, J. Long, I. Korobkov, W. Wernsdorfer and M. Murugeshu, *J. Am. Chem. Soc*., 2011, **133**, 8830; (*c*) S. Ullmann, P. Hahn, L. Blömer, A. Mehnert, C. Laube, B. Abelc, and B. Kersting, *Dalton Trans*., 2019, **48**, 3893; (*d*) L. Zhang, P. Chen, H.-F. Li, Y.-M. Tian, P.-F. Yan and W.-B. Sun, *Dalton Trans*., 2019, **48**, 4324; (*e*) H. Ke, W. Wei, Y.-Q. Zhang, J. Zhang, G. Xie and S. Chen, *Dalton Trans*., 2018, **47**, 16616; (*f*) Q. Zou, X.-D. Huang, J.-C. Liu, S.-S. Bao and L.-M. Zheng, *Dalton Trans*., 2019, **48**, 2735.

23 (*a*) E. L. Gavey, M. Al Hareri, J. Regier, L. D. Carlos, R. A. S. Ferreira, F. S. Razavi, J. M. Rawson and M. Pilkington, *J. Mater. Chem. C*, 2015, **3**, 7738; (*b*) Z. X. Jiang, J. L. Liu, Y. C. Chen, J. Liu, J. H. Jia and M. L. Tong, *Chem. Commun*., 2016, **52**, 6261.

24 (*a*) L. Mandal, S. Biswas, G. Cosquer, Y. Shen and M. Yamashita, *Dalton Trans*., 2018, **47**, 17493; (*b*) R. J. Blagg, L. Ungur, F. Tuna, J. Speak, P. Comar, D. Collison, W. Wernsdorfer, E. J. L. McInnes, L. F. Chibotaru and R. E. P. Winpenny, *Nat. Chem*., 2013, **5**, 673. (*c*) T. Morita, K. Katoh, B. K. Breedlove and M. Yamashita, *Inorg. Chem*., 2013, **52**, 13555.

25 (*a*) M. Ren, D. Pinkowicz, M. Yoon, K. Kim, L.-M. Zheng, B. K. Breedlove and M. Yamashita, *Inorg. Chem*., 2013, **52**, 8342; (*b*) F. Mori, T. Nyui, T. Ishida, T. Nogami, K. Y. Choi and H. Nojiri, *J. Am. Chem. Soc*., 2006, **128**, 1440; (*c*) X.-C. Huang, V. Vieru, L. F. Chibotaru, W. Wernsdorfer, S.-D. Jiang and X.-Y. Wang, *Chem. Commun*., 2015, **51**, 10373; (*d*) Z. Liang, M. Damjanovic, M. Kamila, G. Cosquer, B. K. Breedlove, M. Enders and M. Yamashita, *Inorg. Chem*., 2017, **56**, 6512.

26 (*a*) A. Zouzou, A. Beghidja, J. Long, C. Beghidja, F. Gándara, Y. Guari and J. Larionova, *Dalton Trans*., 2018, **47**, 13647; (*b*) K. R. Meihaus, S. G. Minasian, W. W. Lukens Jr., S. A. Kozimor, D. K. Shuh, T. Tyliszczak and J. R. Long, *J. Am. Chem. Soc*., 2014, **136**, 6056.

27 (*a*) L. Chen, J. Zhou, A. Yuan and Y. Song, *Dalton Trans*., 2017, **46**, 15812; (*b*) P. Kalita, J. Goura, J. M. H. Martínez, E. Colacio and V. Chandrasekhar, *Eur. J. Inorg. Chem*., 2019, 212.

28 M.-E. Boulon, G. Cucinotta, J. Luzon, C. Degl'Innocenti, M. Perfetti, K. Bernot, G. Calvez, A. Caneschi and R. Sessoli, *Angew. Chem., Int. Ed*., 2013, **52**, 350.

Graphical Abstract

for

Exploration of SMM behaviour of Ln$_2$-complexes derived from thianaphthene-2-carboxylic acid

Soumava Biswas,* Leena Mandal, Yongbing Shen and Masahiro Yamashita*
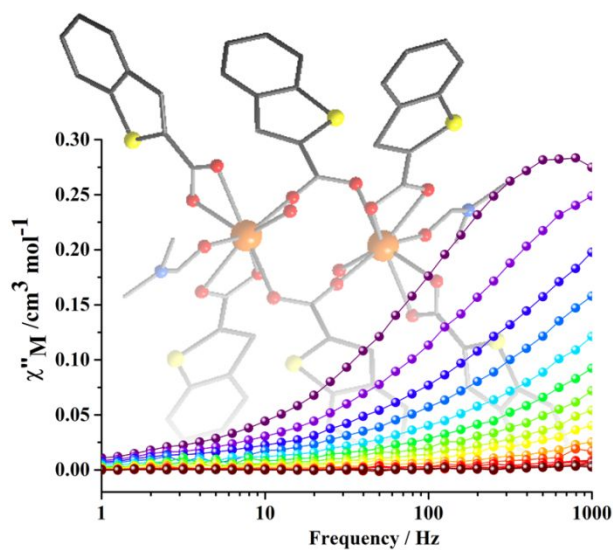
Observation of field induced SMM property of a dysprosium based dinuclear complex derived from thianaphthene-2-carboxylic acid ligand.